GEOPHYSICS, VOL. 85, NO. 2 (MARCH-APRIL 2020); P. D65–D74, 7 FIGS., 1 TABLE.
10.1190/GEO2019-0419.1

DOI:10.1190/geo2019-0419.1

Velocity-attenuation model from check-shot drift trends in North Sea well data

Andrew J. Carter[1], Veronica A. Torres Caceres[1], Kenneth Duffaut[1], and Alexey Stovas[1]

ABSTRACT

Seismic attenuation distorts phase and narrows bandwidth in seismic surveys. It is also an exploration attribute, as, for example, gas or overpressure, may create attenuation anomalies. Compensating attenuation in imaging requires accurate models. Detailed attenuation models may be obtained using full-waveform inversion (FWI) or attenuation tomography, but their accuracy benefits from reliable starting models and/or constraints. Seismic attenuation and velocity dispersion are necessarily linked for causal linear wave propagation such that higher frequencies travel faster than lower frequencies in an attenuative medium. In publicly released well data from the Norwegian North Sea, we have observed systematic positive linear trends in check-shot drift when comparing (lower frequency) time-depth curves with (higher frequency) integrated sonic transit times. We observe velocity dispersion consistent with layers having constant seismic attenuation. Adapting a previously published method, and assuming an attenuation-dispersion relationship, we use drift gradients, measured over thick stratigraphic units, to estimate interval P-wave attenuation and tentatively interpret its variation in terms of porosity and fluid mobility. Reflectivity modeling predicts a very low attenuation contribution from peg-leg multiples. We use the attenuation values to develop a simple regional relationship between P-wave velocity and attenuation. Observed low drift gradients in some shallower units lead to an arch-shaped model that predicts low attenuation at both low and high velocities. The attenuation estimates were broadly comparable with published effective attenuation values obtained independently nearby. This general methodology for quickly deriving a regional velocity-attenuation relationship could be used anywhere that coincident velocity models are available at seismic and sonic frequencies. Such relationships can be used for fast derivation (from velocities) of starting attenuation models for FWI or tomography, constraining or linking velocity and attenuation in inversion, deriving models for attenuation compensation in time processing, or deriving background trends in screening for attenuation anomalies in exploration.

INTRODUCTION

Wave attenuation affects all seismic data, reducing the bandwidth and seismic amplitudes with propagation distance and causing time and phase shifts. It is often accounted for in seismic time processing using a single Q value — an "effective Q" from seabed to reservoir depths. Attenuation estimates from surface and borehole seismic exhibit a trade-off between resolution and accuracy (White, 1992). Although smooth background Q models are routinely derived, obtaining models with sufficient resolution and accuracy to link reliably to geologic variation remains challenging. Robust empirical relationships between measured values, such as instantaneous P-wave velocity and attenuation, would aid in the fast derivation of background models and identification of attenuation anomalies that may be associated with, for example, overpressured zones (Carcione and Helle, 2002) or the presence of gas (Klimentos, 1995). Stewart et al. (1984) relate seismic dispersion, quantified via drift between check-shot and integrated sonic traveltimes, to attenuation. The resolution in attenuation thus obtained is limited by different factors than in amplitude-based methods, and in favorable circumstances may allow investigation of attenuation in thick geologic formations. Similar methods have been applied by De et al. (1994), Tezuka and Takahashi (1993), and several others, although this method for Q estimation is not routinely used in industry.

We apply Stewart et al.'s (1984) method to borehole data from 15 wells from the Norwegian sector of the North Sea. The resulting

Manuscript received by the Editor 28 June 2019; revised manuscript received 24 September 2019; published ahead of production 16 December 2019; published online 25 February 2020.
[1]Norwegian University of Science and Technology (NTNU), Department of Geoscience and Petroleum, S. P. Andersens veg 15a, Trondheim 7031, Norway. E-mail: andrew.j.carter@ntnu.no; veronica.a.t.caceres@ntnu.no; kenneth.duffaut@ntnu.no (corresponding author); alexey.stovas@ntnu.no.

DOI:10.1190/geo2019-0419.1

effective Q values from seabed to reservoir depths are in broad agreement with the lower of the values published for nearby parts of the North Sea by Strijbos et al. (1998). Within stratigraphic groups of sufficient thickness, we estimate the interval drift gradient and thus the interval effective Q^{-1}. We model to assess the contribution to drift of pulse broadening due to scattering in fine layering (O'Doherty and Anstey, 1971) at one of the wells, and we use 14 of the wells to derive a preliminary regional relationship between the attenuation and the P-wave interval velocity at seismic frequencies. This arch-shaped relationship differs significantly from most published observations of the relationship between attenuation and P-wave velocity in which attenuation tends to decrease monotonically with increasing P-wave velocity (e.g., Waters, 1981; Koesoemadinata and McMechan, 2001). We propose a tentative interpretation of this difference. The model is used to predict attenuation and drift at a blind well, producing a reasonable prediction.

METHODS

Attenuation estimation from drift

It has been shown that for linear wave propagation, with causality applied as a constraint, seismic attenuation and velocity dispersion are mathematically linked (for a review, see, e.g., Aki and Richards, 1980). Thus, we cannot have attenuation without velocity dispersion and vice versa. Choice of a form for the velocity dispersion is therefore equivalent to choosing a frequency dependence of attenuation, and a formula that specifies the attenuation and dispersion in an attenuative medium is known as an attenuation-dispersion pair.

An example is the Kolsky-Futterman attenuation-dispersion pair (equation 1; Kolsky, 1956; Futterman, 1962) that, although strictly applying to phase velocities, is given here because it approximately applies to the group velocity (as shown by Stewart et al., 1984):

$$\frac{V_{\mathrm{P1}}}{V_{\mathrm{P2}}} = 1 + \frac{1}{\pi Q}\ln\left(\frac{f_1}{f_2}\right), \tag{1}$$

where V_{P1} is group velocity at frequency f_1 and V_{P2} is group velocity at frequency f_2 for P-wave propagation in a homogeneous anelastic medium with intrinsic attenuation Q^{-1}.

The existence of such relationships between attenuation and dispersion means that, in principle, assuming an attenuation-dispersion pair that adequately describes the total attenuation and dispersion over the bandwidth of interest can be identified, measurements of attenuation can be derived from measuring velocity dispersion, and vice versa. Sometimes estimates of dispersion made from the same data as attenuation estimates can be used either to (slightly) improve inversion for attenuation parameters (Rickett, 2007), or they may be used as a quality control step on attenuation estimates from seismic data, to identify, for example, problems resulting from tuning or interference.

Given that a relationship between velocity dispersion and attenuation exists, it has long been recognized that the difference (known as check-shot drift) in seismic velocities observed by sonic logs, acquired in the kHz range, and borehole seismic surveys, acquired at tens of Hz, may contain useful information about seismic attenuation (Strick, 1971). Although other factors also influence check-shot drift and these have been listed and studied in detail by other authors (Goetz et al., 1979; Stewart et al., 1984), we seek to use check-shot drift as a quick method to derive an approximate regional relationship between attenuation and velocity from publicly released well data.

We modified a published approach (Stewart et al., 1984) based on comparing time-depth pairs from check shots and vertical seismic profiles (VSPs) with integrated sonic log traveltimes. We make no distinction between released time-depth curves derived from check shots and those from zero-offset VSPs; all are referred to in this paper as check-shot data. All of the wells studied are exploration wells. Most of the wells are close to vertical and have a maximum deviation of 6°; three wells have a deviation of between 6° and 13° for parts of the wellbore. Drift curves thus obtained are positive when the sonic has traveled faster than the direct P-wave arrival from the check-shot survey. Assuming that other factors contributing to the drift are small, the following equation, derived from Stewart et al. (1984), can be used to estimate Q^{-1} from the drift gradient $\Delta\mathrm{drift}/\Delta z$:

$$\frac{1}{Q} = \frac{\pi}{\ln\left(\frac{f_2}{f_1}\right)}\left[1 - \frac{1}{\left(V_{\mathrm{P}_{0f2}}\frac{\Delta\mathrm{drift}}{\Delta z} + 1\right)}\right], \tag{2}$$

where $\Delta\mathrm{drift} = \Delta t_{\mathrm{Check-Shot}} - \Delta t_{\mathrm{IntegratedSonic}}$, measured over a depth interval of thickness Δz, f_2 is the sonic frequency, f_1 is the dominant frequency of the check shot, and $V_{\mathrm{P}_{0f2}}$ is the vertical P-wave sonic velocity derived from the reciprocal of the average slowness over depth interval Δz. Here, accuracy is limited by the use of released well data, which do not include the check-shot first-arrival waveforms themselves, nor the raw sonic waveform data. This presents challenges for evaluating accuracy and uncertainty because we lack accurate values for f_1 and f_2, check-shot traveltime picking errors, information on the picking method (e.g., crosscorrelation), the phase picked (e.g., trough-trough or onset), as well as information about the verticalization of the traveltimes and the local geologic structure around the well. The quality of the sonic log may also be difficult to assess.

Our minor modification to Stewart et al.'s (1984) method is in estimating drift gradients for consistently chosen (thick) geologic intervals, using a linear regression of all drift values within each interval of interest. An uncertainty in the drift gradient is obtained based on χ^2 minimization (see Appendix A), and this is the source of the error bars on our Q^{-1} estimates used as weights in the weighted least-squares nonlinear regression to derive the velocity-attenuation model.

Uncertainties, particularly in the picking of the time-depth curves, but also in the sonic transit times and other parameters, lead to a trade-off between resolution and accuracy in our Q^{-1} estimates. Following Stewart et al. (1984), when $(1/\pi Q)\ln(f_1/f_2)$ is small, equation 2 can be approximated as

$$\frac{1}{Q} \approx \frac{\pi V_{\mathrm{P}_{0f2}}\frac{\Delta\mathrm{drift}}{\Delta z}}{\ln\left(\frac{f_2}{f_1}\right)}, \tag{3}$$

from which we can see that the magnitude of the drift accumulated within a layer, $\Delta\mathrm{drift}$, is approximately proportional to $\Delta t/Q$, where Δt is the vertical one-way traveltime through the layer (equivalent to $\Delta z/V_{\mathrm{P}_{0f2}}$). Therefore, the relative magnitude of the errors on the drift compared to the true magnitude of $\Delta t/Q$ controls the resolution that can be accurately obtained in Q^{-1} estimates. In other words, the less attenuative a layer is, the thicker it needs to be, or the smaller the uncertainty on the drift measurements required,

for an accurate estimate of Q^{-1}. However, in practice, the true magnitude of $\Delta t/Q$ is unknown a priori, as is the uncertainty on the drift, so we chose to set a limiting threshold on the layer thickness such that we seek to estimate Q^{-1} from drift only in layers with drift measurements covering a thickness of at least 250 m. We chose this threshold empirically because for typical check-shot and sonic frequencies, and a typical interval Q value of 100, a 250 m layer thickness is sufficient to accumulate more than 2 ms of drift, which appears to be greater than the noise level in the drift. A depth interval of 250 m usually also contains several points in the time-depth curve. More time picks are desirable to improve the accuracy and precision of the regression-based estimate of the drift gradient. To meet this thickness threshold, some geologic intervals that are thin but that exhibit similar geologic characteristics and similar drift gradient are grouped together for analysis, whereas other relatively thin layers that differ from their neighbors are excluded from the analysis.

Figure 1 uses well 34/7-1 to illustrate the method and shows example Q values. The process that is followed essentially progresses from left to right in this figure.

- Available well-log data and the time-depth curve for a well are plotted, well reports are obtained, and these are used for basic quality control of the sonic and time-depth curves. Well logs such as gamma ray, density, resistivity, and the caliper are also used in interpretation of the results.
- The drift is calculated by subtracting the accumulated integrated sonic transit times measured relative to the first good time-depth point within the range covered by the sonic log from the accumulated check-shot traveltime. A least-squares linear regression for the overall drift gradient followed by application of equation 2 gives a rough estimate of the overall level of attenuation in the well.
- The well is split into intervals based on thick geologic groups, and a linear regression is performed for each interval's drift gradient and its uncertainty. Here, the drift and its gradient are calculated using integrated sonic transit times relative to the first good time-depth point in the interval.
- The interval drift gradients and their uncertainties are converted into Q^{-1} values with the uncertainties (see equation 4) derived based on propagation of error formulas (see Appendix B). In our figures, we display Q^{-1} because this is the property that we are measuring, but we annotate Q values becasue these numbers are more familiar to practising geophysicists.

Based on equation 2, and assuming that the uncertainty on the sonic velocity is relatively small $\sigma^2_{(V_{P0f2})} \approx 0$ and that f_1 and f_2 are known and constant, therefore their ratio (f_1/f_2) is also constant, the variance on Q^{-1}, $\sigma^2_{(Q^{-1})}$ will depend only on the drift gradient variance $\sigma^2_{(\Delta\text{drift}/\Delta z)}$:

$$\sigma^2_{(Q^{-1})} \approx \left[\frac{\pi V_{P0f2}}{\ln\left(\frac{f_2}{f_1}\right)\left(V_{P0f2}\frac{\Delta\text{drift}}{\Delta z}+1\right)^2}\right]^2 \cdot \sigma^2_{\frac{\Delta\text{drift}}{\Delta z}}. \quad (4)$$

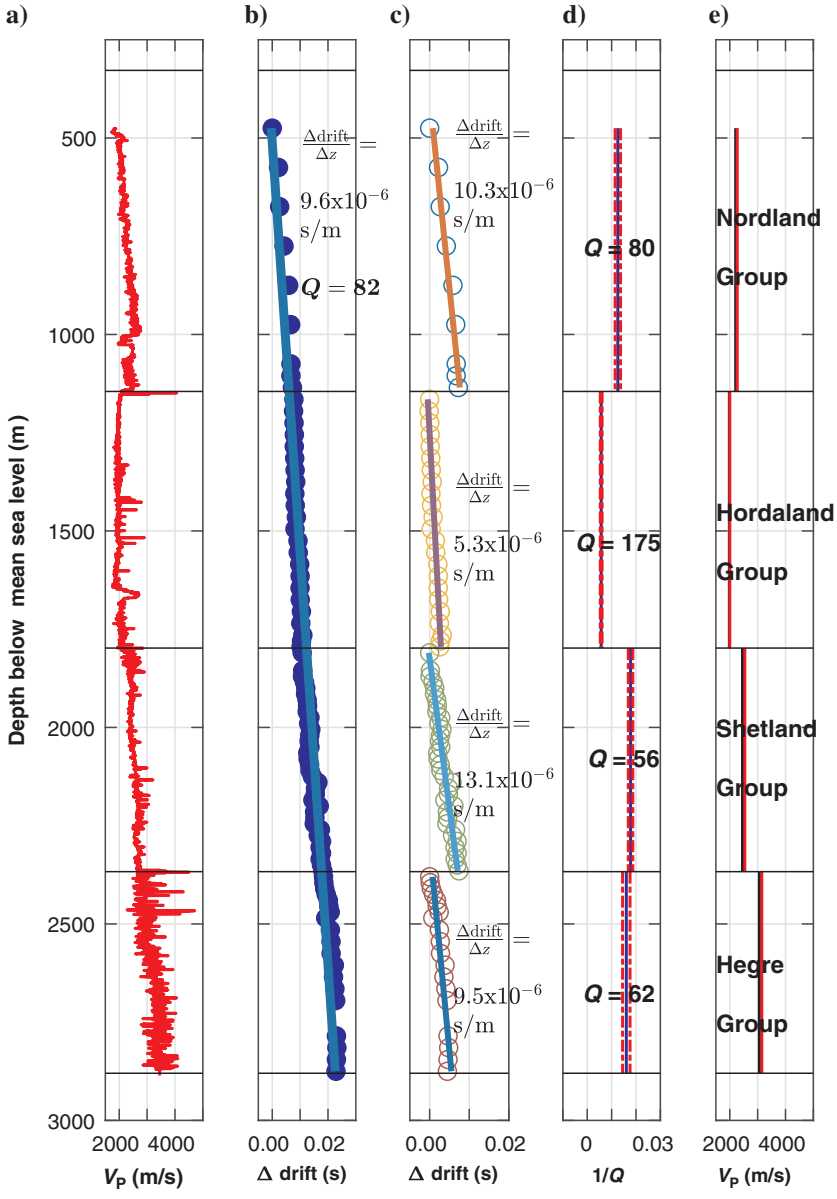

Figure 1. Example well: 34/7-1: Derivation and QC of drift and Q^{-1} estimates: (a) sonic log, (b) check-shot drift estimates (blue circles) and average drift gradient (blue-green line) estimated by least-squares linear regression, and (c) drift gradient estimation for individual geologic groups. Approximate uncertainties, not shown, on the drift gradients are derived via χ^2 minimization. (d) Interval attenuation estimates for each geologic group (blue lines) with the standard deviations in Q^{-1} (red dotted lines) derived from uncertainties in drift gradients. The corresponding interval Q values are annotated. (e) Interval vertical P-wave velocity derived from sonic (red) and check shot (black) for each geologic group. All five panels share a common depth axis and zonation into geologic groups.

Figure 1e is included to illustrate the magnitude of the velocity dispersion between the check-shot and sonic velocities that is consistent with the drift gradients and Q^{-1} estimates obtained.

Similar analyses were applied to data from 14 other wells. Data from a further two wells were examined but excluded from the study (see Table C-1).

The contribution of scattering in our study area

We evaluated the contribution of scattering to dispersion and attenuation at one well (34/7-1). Assuming that scattering attenuation and intrinsic attenuation are approximately additive (Richards and Menke, 1983), we use a Kennett-Bouchon reflectivity modeling code (SKB2) (Dietrich, 1988) on logs blocked with a 4 m Backus average, modeling with almost zero attenuation ($Q = 10{,}000$), and measuring drift on the synthetic zero-offset vertical seismic profiles. The results of, and synthetic data used in, this analysis are summarized in Figures 2, 3, and 4. A broadly similar approach to model drift has been used by Sato et al. (2000).

Figure 4 shows that the likely contribution to dispersion in this region from the type of scattering studied by O'Doherty and Anstey (1971) is very small. It is unlikely to be significantly larger in our other wells because the strength of the acoustic contrasts in fine layering is relatively small in this geologic setting. Low levels of scattering attenuation were also reported recently using slightly different methods on a VSP from well 16/23-7 in the Kinnoull Field in the central North Sea by Beckwith (2017). It remains possible that other types of scattering, as studied by Worthington and Hudson (2000), contribute dispersion or otherwise bias our analyses and are thus a potential source of noise remaining unaccounted for in our results, but we lack information about the geologic structure, particularly fault and fracture zones in close proximity to our wells, with which to attempt to assess this. We used the same modeling method to create synthetic data including attenuation to check the accuracy of our drift analysis implementation.

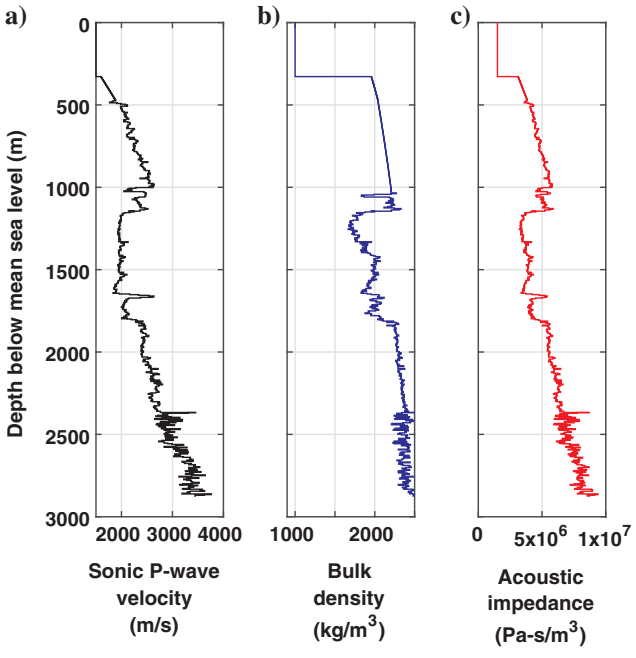

Figure 2. Models based on 4m blocked Backus averaged logs from well 34/7-1 used in modeling the likely impact of layer-induced scattering on drift: (a) V_P model, (b) density model, and (c) acoustic impedance model.

Geologic setting of the northern North Sea area

The study area is within the Norwegian part of the northern North Sea with wells located between 60°N and 62°N that penetrate sediments of Cenozoic and Mesozoic age. Most of the prolific reservoirs in the area are in Middle Jurassic to upper Triassic sandstones with average porosities between 20% and 30% and average thicknesses of approximately 50 m. These sandstones are interbedded with clay-

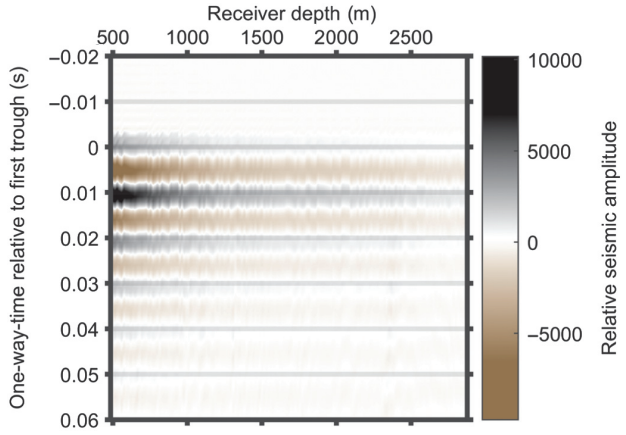

Figure 3. Synthetic zero-offset VSP data based on reflectivity modeling with the first arrivals flattened on the first trough pick.

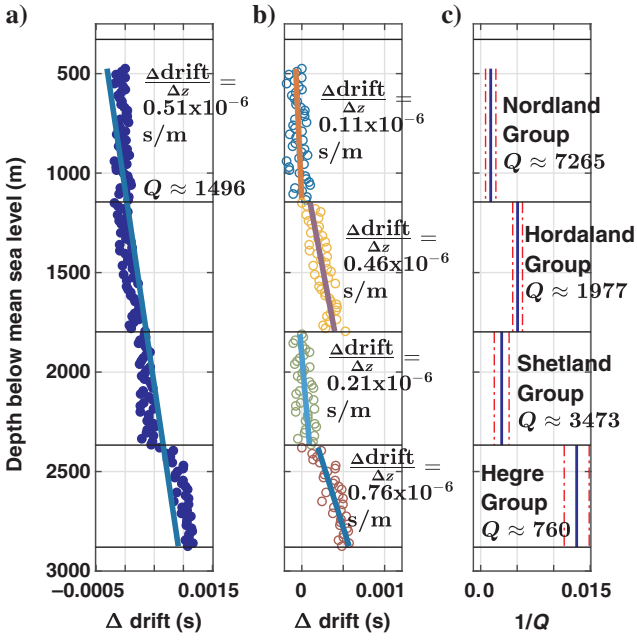

Figure 4. Check-shot drift analysis on the modeled data with resulting Q^{-1} estimates: (a) relative drift curve with linear regression fit over the whole VSP depth range, (b) relative drift within each geologic group with regression lines fitted per group, and (c) interval Q^{-1} estimates ± 1 s.d. obtained using the regressions from the center panel in combination with equation 2.

DOI:10.1190/geo2019-0419.1

stone, composed of clay and silt, where clay constitutes the largest part of the rock matrix. The lithostratigraphic groups covering these units are the Hegre, Statfjord, Dunlin, and Brent Groups representing the sand-rich groups, whereas the late Jurassic Viking Group is mainly composed of organic-rich shales. These Triassic and Jurassic sediments are overlain by the Cretaceous Cromer Knoll and Shetland Groups and the Tertiary Rogaland, Hordaland, and Nordland Groups, which are, in general, characterized by widespread deposition of mainly calcareous claystones and marls in the Cromer Knoll Group and claystone (clay and silt) in the rest of the stratigraphic groups in the area (Isaksen and Tonstad, 1989; Thyberg et al., 2000; Storvoll et al., 2005; Marcussen et al., 2009). Sand-rich rocks of Cretaceous and Tertiary age constitute only a small proportion of the stratigraphic groups. In terms of clay mineralogy, the claystones near the top of the Rogaland Group become increasingly tuffaceous due to deposition of volcanic ash from volcanic activity during the opening of the North Atlantic Ocean in the early Tertiary (Isaksen and Tonstad, 1989; Thyberg et al., 2000). Later erosion of these volcanic deposits led to the deposition of relatively smectite-rich claystones within the lower part of the Hordaland Group (Thyberg et al., 2000; Marcussen et al., 2009) that are associated with lower bulk rock densities compared to the surrounding clay-rich rocks. This is related to the fact that smectite is associated with the highest porosities among the clay minerals (Mondol et al., 2007), although the permeability of the smectite is very low. Toward the top of the Hordaland Group, the claystones are classified as ooze-rich claystone due to the high content of skeletal material also associated with high porosities (Øygarden et al., 2015), but not necessarily high permeabilities.

RESULTS

The results of the drift analysis applied to 15 wells are plotted in Figure 5. Intervals below our 250 m threshold thickness are excluded, as are intervals where the sonic has been affected by poor borehole conditions resulting in great uncertainty in the Q^{-1} estimates. Where wells contained intervals with zones of unexplained negative drift or rapidly varying or unstable drift gradient, we excluded them from our analysis. A list of excluded data by well and geologic group, with the exclusion criteria applied, is provided in Appendix C.

We sought to account for the data shown in Figure 5 using a simple robust empirical model (shown in blue in the figure), with as few parameters as possible, that could be of use in predicting attenuation from velocities at seismic frequencies. We therefore chose a model of the form of equation 5:

$$\frac{1}{Q} = a_0(V_{P_0} - V_{P_0\,\mathrm{min}})(V_{P_0\,\mathrm{max}} - V_{P_0}), \tag{5}$$

where a_0, $V_{P_0\,\mathrm{min}}$, and $V_{P_0\,\mathrm{max}}$ are the nonlinear weighted least-squares fitted parameters representing an attenuation scale factor and the limiting velocities of the model. The values obtained for a_0, $V_{P_0\,\mathrm{min}}$, and $V_{P_0\,\mathrm{max}}$ are $1.084\times10^{-8}\pm3.214\times10^{-9}\,\mathrm{s^2/m^2}$, $1644\pm114.5\,\mathrm{m/s}$, and 4332 ± 287.7 m/s, respectively. V_{P_0} is the velocity derived from the time-depth curve, i.e. from VSP or checkshot data. The uncertainties are standard errors. The method used for the regression is briefly summarized in Appendix A. Figure 6 shows that the regional model (derived from 14 wells including well 34/7-1) generally does a good job of predicting the drift and attenuation at a blind well (well 34/8-6) apart from the Rogaland Group, where the data exhibit less drift than predicted by the model. While our model would benefit from the inclusion of more well data, especially at intermediate velocities, we include the values that we obtained for the model parameters to allow the reader to plot their own North Sea attenuation estimates against the model predictions or to test the use of the model on their own data.

DISCUSSION

We interpreted a general trend in the data. This is an arch-shaped model that predicts Q^{-1} from vertical P-wave interval velocities derived from released time-depth curves for wells in the database of the Norwegian Petroleum Directorate. The shallowest stratigraphic groups have low to moderate attenuation values. The Hordaland Group, however, has the lowest attenuation. This may be controlled by the clay mineralogy. Although the Shetland and Viking Groups are older and deeper formations than the Nordland and Hordaland Groups, they are located at the apex of the arch, exhibiting the highest attenuation values. There is, though, significant scatter in the Q^{-1} values obtained for rocks with this intermediate velocity range in the model. In this region, the Shetland and Viking Groups are often very likely to be overpressured and may also contain source rocks (Evans, 2003). Finally, the deepest stratigraphic groups show moderate to low attenuation, which decreases as their burial depth and P-wave velocity increase.

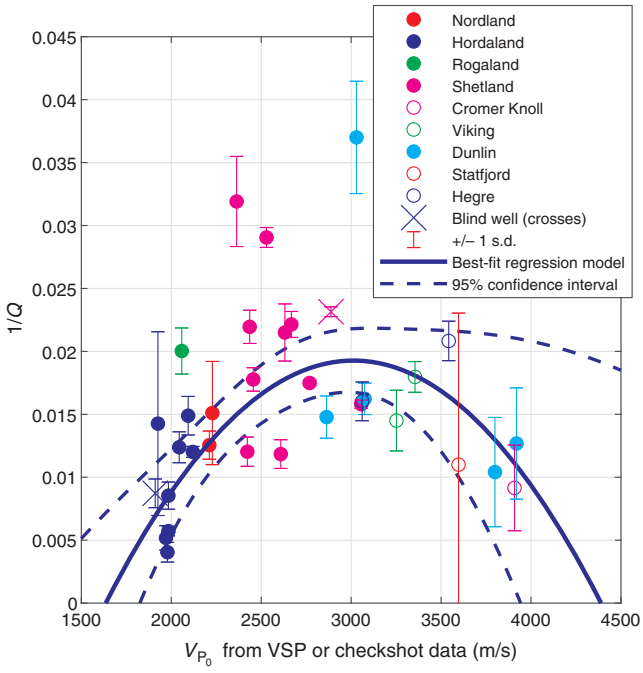

Figure 5. Regional model relating attenuation (Q^{-1}) to verticalized P-wave velocity from check shots in the Norwegian sector of the North Sea. The Q^{-1} values shown for each interval (color-coded by geologic group) are estimated from check-shot drift measurements from 15 wells. The central blue solid line is a model (equation 5), from a nonlinear least-squares fitting of observed data, whose fitted parameters are given in the text. The dashed blue lines represent 95% confidence intervals on the fitted model, and the error bars on the individual points are derived from least-squares regression estimates of the drift gradient. Attenuation estimates from the blind well (34/8-6) were not included in the regression but are displayed with crosses.

Mineralogical effects

The Hordaland Group consists mainly of mudstones with some sand/siltstones and limestone/dolomite stringers. Intrinsic attenuation driven by the combination of mineralogical composition and fluid effects can potentially explain the obtained results. This stratigraphic group exhibits distinctive patterns in its wireline log suite with low P-wave velocity (see Figure 1), high porosity, low resistivity, and low density. The Hordaland Group differs in clay mineralogy and clay content from the Nordland Group above and the Shetland Group below. In our study area, the mudstone has a considerable increase, from 5%–10% to 60%–80%, in smectite content between the Nordland and Hordaland Groups.

In general, the density-depth trend exhibited by the Hordaland and Rogaland Groups is fairly consistent with Mondol et al.'s (2007) experimental mechanical compaction of brine-saturated smectite where the bulk densities are as low as 1.8–2.0 g/cm^3 down to approximately 2 km in depth. Areas where the bulk density is lower than expected could be due to overpressured zones. However, clay mineralogy effects may dominate, but they may appear as overpressure because smectite-rich mudstones are characterized as extremely fine grained, with low permeability and very high water content due to their large clay surface area, making them less prone to mechanical compaction (Marcussen et al., 2009).

Our lowest Q^{-1} estimates are observed in the Hordaland Group in Figure 5. This stratigraphic unit is mainly mudstone dominated with high smectite content appearing as a soft formation with high porosity and fluid content. As a consequence, the low-permeability smectite-rich mudstone may be a major contributor to the low attenuation response observed due to the immobility of free water at low frequency and mesoscopic scales. Although attenuation and dispersion mechanisms are frequency dependent, Batzle et al. (2006) propose from laboratory experiments made within the seismic frequency band (1–1000 Hz) that fluid mobility is a key factor that controls pore fluid motion and pore pressure in a porous medium. For example, for low fluid mobility, the relaxation times needed for fluid equilibration will be longer, lowering the dispersive frequency band. For this reason, many sedimentary rocks fall into the so-called high-frequency regime even in the typical seismic frequency bandwidth. Hence, local flow mechanisms that cause attenuation can occur due to mesoscale heterogeneities in porous media. In other words, the attenuation and dispersion response in the seismic, sonic, and ultrasonic frequencies can have similar behavior. For the Hordaland Group, the smectite-rich mudstone, it is very likely that the low permeability reduces fluid mobility and it is possible that the dispersive frequency band is below the seismic frequency bandwidth. Hence, velocity dispersion and attenuation between the seismic and ultrasonic frequencies can be almost negligible, as shown by Batzle et al. (2006).

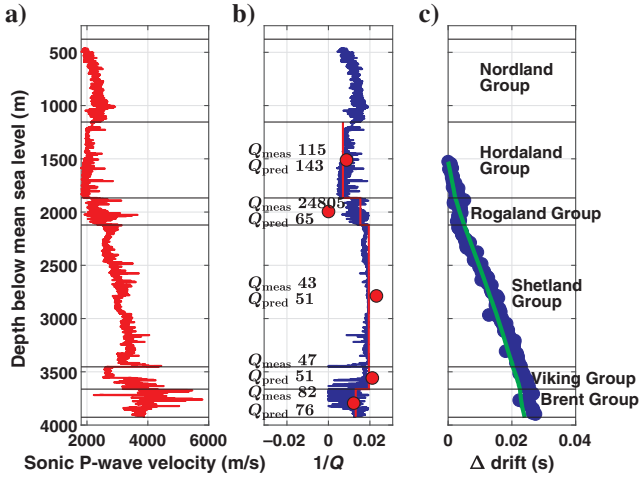

Figure 6. Well panel comparing the model predictions from Equation 5 with measurements from the blind well (34/8-6): (a) P-wave sonic, (b) predicted attenuation log (blue); this is based on the sonic log and a combination of equations 5 and 1; interval Q^{-1} predictions (red lines) based on interval vertical check-shot velocities inserted directly into equation 5; drift-based Q^{-1} measurements (red circles), and (c) predicted drift (green line) and measured drift (blue circles). No good check-shot data were available to quantify drift in the Nordland Group for this well.

Overpressure and partial saturation effects

The Shetland Group's overpressure has been reported as likely being associated with posterior sedimentation processes (Wensaas et al., 1994), which means that this stratigraphic unit was deposited in a normal compaction regime. Buildup of anomalous pore pressure has likely occurred after deposition of a Paleocene seal followed by high sedimentation rates during the late Tertiary. Local hydrocarbon leakage from older Jurassic reservoirs got trapped in the Upper Cretaceous sediments. In addition, microcracks and fractures are likely to be present (Wensaas et al., 1994).

The higher attenuation values observed for the Shetland Group might be intuitively associated with overpressure zones and associated fracturing. Similarly, as we move deeper into the section, the temperature increases and this triggers the start of chemical compaction and mineralogical transformations. Thyberg et al. (2010) show how smectite to illite transformation of the illite-smectite (I/S) mixed layers at 60°C–100°C during progressive burial leads to the expulsion of water and silica. The expelled water impacts the ion concentration of the connate water within the formation, reducing its salinity while increasing the resistivity log response. The expelled silica contributes to microcrystalline quartz cementation that stiffens the rock and reduces its permeability. This is observed as increasing density and velocity at depths greater than 2.5 km. Under these conditions, one might expect low Q^{-1} values, but we have observed a range of Q^{-1} values. The overpressure buildup could explain the higher attenuation values considering the effect of fractures allowing fluids to flow.

The Draupne Formation, which makes up parts of the Viking Group in the North Sea, is a regional source rock. Hence, it contains adequate volumes of organic matter that in certain areas cause pore pressure buildup and microfracturing due to the transformation of kerogen to oil and/or gas. High attenuation estimates for this unit are possibly related to this process and the presence of residual hydrocarbons. The latter is one of the main causes of attenuation previously studied by White (1975), Dutta and Seriff (1979), and Klimentos (1995).

Burial depth effects

For deeper sediments, such as the reservoir rocks within the Brent, Dunlin, Statfjord, and Hegre Groups, Q^{-1} ranges from moderate to low. This is mainly due to their greater burial depth that results in reduced porosity and permeability caused by cementation due to a temperature regime likely greater than 75°C. Lower porosity implies

stiffer and more consolidated rocks. Hence, attenuation related to fluid flow is expected to be low. The reservoir units in our study area are more complex because several factors may influence the attenuation estimates, for example, the presence of hydrocarbons and multiphase saturation, variation in clay content, porosity, and permeability.

Comparison with published North Sea Q values

Figure 7 shows a map that includes, annotated in black, Q values published by Strijbos et al. (1998) from the UK sector of the North Sea. Their values were obtained using a well-tie optimization process and are assumed to represent effective Q from the seabed to the top reservoir. Effective Q values from our study are annotated in blue text. These have been calculated based on the difference in drift between the shallowest depths included in our analyses and the drift at the top reservoir, and they have been extended to the seabed, assuming that the interval Q value for the uppermost geologic group for each of our wells continues to the seabed. The same procedure to calculate effective Q was followed using the predicted drift curve from the model applied to the blind well. This is, therefore, rather an approximate comparison, but it does show that our approach is giving Q values comparable to, though on the low side of, those published by Strijbos et al. (1998). Only wells with consistently positive drift gradients in all of the geologic groups above the top reservoir, typically the uppermost Jurassic sands, were included in this comparison. Unfortunately, the two wells in this comparison that are closest together geographically are located in an area in which the bathymetry is varying relatively quickly laterally, and this may have some influence on these two values in the northwest of the map.

Key assumptions

The single biggest assumption in our method is our choice of the Kolsky–Futterman attenuation-dispersion pair (equation 1; Kolsky, 1956; Futterman, 1962). We have made a pragmatic choice of this attenuation-dispersion relationship for simplicity's sake and because we are currently not aware of one single alternative that would be preferable for the range of mixed lithologies, pore pressures, and fluid saturations encountered in our study region. Our chosen attenuation-dispersion pair implies that Q is independent of frequency and does not represent a single physical attenuation mechanism, but it might roughly approximate the combined effect of a band of mechanisms with attenuation peaks at different frequencies (Liu et al., 1976). A similar frequency dependence of Q might also be observed due to scattering from fine layering with a fractal distribution (van der Baan, 2002), although for the wells we studied, we believe that the contribution from layer-induced scattering is small.

An approximately frequency-independent Q has often, though not always, been observed on VSP and check-shot data when measurements have been made robustly over relatively large depth ranges (Raikes and White, 1984), although these are generally estimates of effective Q, that is with scattering effects included. Effective Q approximately independent of frequency has also been observed to some extent on deghosted surface seismic (Vigner et al., 2010) and in Q estimates, which allowed for the frequency dependence of Q, from surface seismic (Beckwith et al., 2017) and VSP data (Beckwith, 2017) from the central North Sea.

We note, however, that over smaller depth ranges it can be practically impossible to distinguish between different attenuation models and their corresponding mechanisms from field data (Toverud and Ursin, 2005) and that there are several plausible attenuation and scattering mechanisms that should lead to frequency-dependent attenuation (Gurevich and Pevzner, 2015). Though our choice of attenuation-dispersion model is theoretically unattractive with respect to expectations from poroelasticity, we are not currently aware of a more appropriate assumption to make on frequency-dependence of Q and the accompanying dispersion, which is supported by evidence based on field measurements (i.e., evidence acquired in situ in which waves at seismic frequencies sample heterogeneity over the relevant range of scales).

We note that it is not necessary for the dispersion to be correctly described over the entire frequency range, nor is it necessary for Q at sonic frequencies to match Q at seismic frequencies for this to be a useful practical approach. All that is necessary is that the magnitude of total dispersion from seismic to sonic frequencies is a good and consistent predictor of dispersion within the seismic bandwidth. This is important because attenuation can often be significantly higher when measured from full-waveform sonic than from surface seismic (Houck, 1987; Neep, 1995), and this implies that dispersion in the kHz range is higher than dispersion in the seismic bandwidth. If we had access to the waveforms used to derive the time-depth curves, we could test this directly by looking for dispersion within the bandwidth of the check shot (Rappin and Barnes, 2008). However, if the Q^{-1} values derived from the drift agree with the Q^{-1} derived from established methods, then our assumption is also, indirectly, validated. Our general methodology could easily be adapted

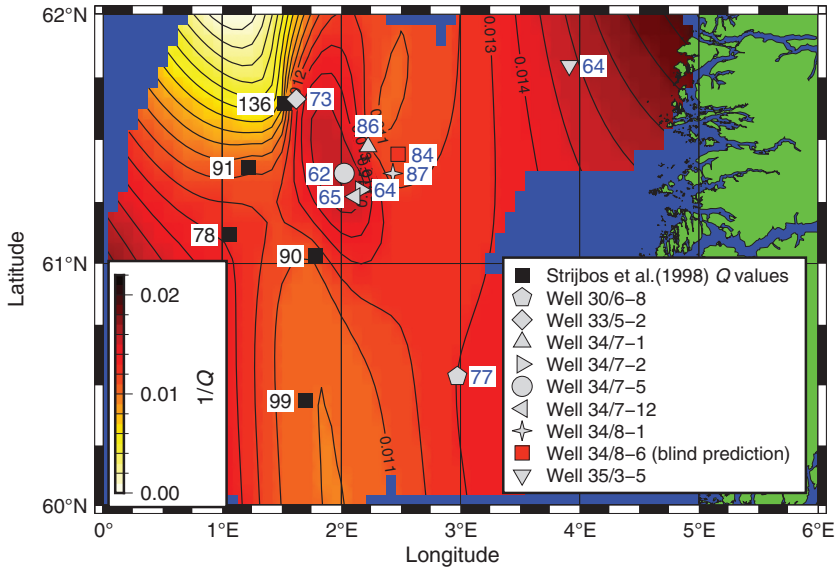

Figure 7. Comparison of nearby published effective Q values (black squares) from Strijbos et al. (1998) with comparable values from our study (gray symbols). These are overlain on a contour map of attenuation (Q_{eff}^{-1}) based on the same values. The value predicted using equation 5 at the blind well is also plotted as a square with the color corresponding to its Q^{-1} value.

DOI:10.1190/geo2019-0419.1

to use any attenuation-dispersion pair of the reader's choice and even to vary this choice by geologic interval.

We have also assumed that where drift is stable and positive that it is mostly caused by dispersion related to seismic attenuation. There are many factors that can influence check-shot drift locally and bias it in either a positive or a negative direction. These have been studied previously (Stewart et al., 1984), and these issues are probably responsible for attenuation estimation from drift not being in common use. The focus of this study has not been to investigate the biases on check-shot drift, but to investigate whether a simple analysis, based on data in the public domain, has the potential to produce useful results.

Our empirical model relates attenuation (Q^{-1}) to the P-wave interval velocity only for consolidated sediments in the region studied. In practical use of the attenuation models, it may be necessary to extend the model to the seabed. Our results give no information about what happens at shallower depths than those included in our data sets, beyond the limiting velocities in our model, and in unconsolidated sediments and suspensions. It is by no means our intention to imply that intrinsic attenuation is necessarily zero either at the seabed or at great depth. The reader wishing to extrapolate the attenuation model to the seabed is directed to published work on Q estimates in shallow marine sediments (Pinson et al., 2008; Zhou et al., 2009).

Intrinsic attenuation at velocities higher than those included in our model is likely to be very low, due to the limited opportunities for mesoscopic wave-induced fluid flow at depth and in the hardest rocks. There is still likely the potential for scattering attenuation related to layering, and to fault zones and fracturing, the magnitude of which can be estimated using methods such as those used by Worthington and Hudson (2000).

APPLICATION OF THE RESULTS AND METHODOLOGY

Potential applications of our general methodology might be to derive empirical relationships between attenuation and velocity (or other measurables) in other study areas. These empirical relationships can then be smoothed and used locally in Q compensation or to provide initial models for Q tomography or for viscoacoustic or viscoelastic full-waveform inversion (FWI), either to provide initial models or to reduce the number of parameters in the initial inversion iterations. Large-scale systematic, and perhaps automated, application of the method could be used to build an understanding of geologic controls on seismic attenuation as observed in reflection seismic data. Predictive models thus derived could also be compared with results from viscoacoustic FWI and attenuation tomography to identify anomalous zones, which may then need to be analyzed in terms of factors such as fluid type and saturation, pore pressure, fluid mobility, source rock maturity (if applicable), and potential for scattering attenuation from fine-layering, faulting, or fracturing.

CONCLUSION

We interpret the rising limb of our "arch" model for low velocities, due to low drift in the Nordland and Hordaland Groups, as being due to a combination of soft material with high porosity (brine constitutes a large part of the rock volume) and low permeability such that the fluid contained in the rock is not free to move in response to the passing of a seismic wave. We interpret the decrease in attenuation for high velocities (>3000 m/s) to be due to a reduction in wave-induced fluid flow as porosity decreases with depth and as the matrix and pores become stiffer and harder to deform due to compaction. More data are needed to better constrain the model between 2500 and 3500 m/s, but some of the variation in drift in this velocity range is likely to be due to overpressure and the presence of hydrocarbons and source rocks. These variations, when better understood, may allow the model to be used to identify anomalous zones.

We identified systematic linear drift trends in the North Sea. We interpreted these in terms of the regional geology, assuming the drift to be mostly due to dispersion from anelastic attenuation, having so far found the contribution from scattering attenuation to be very small. The method assumes a simple phenomenological attenuation-dispersion relationship that does not correspond to a single physical attenuation mechanism. Other full-bandwidth attenuation-dispersion models could also potentially be used. Different models could be used for different lithology and fluid types to account for expected mechanisms. Our model predicts effective Q-values of a reasonable magnitude when compared with values reported in the literature for the UK side of the northern North Sea. Analysis of more well data from this region, particularly check-shot waveform data, would allow us to further develop, constrain, and understand our model, particularly its attenuation predictions for intermediate P-wave velocities (the top of our arch). We may then further evaluate its predictive capacity and usefulness in a variety of applications within seismic processing, modeling, and inversion. We believe that the general approach that we have taken might also be useful for developing Q-velocity relationships in other regions.

ACKNOWLEDGMENTS

We would like to thank the Norwegian Petroleum Directorate for making the data available for this study. We acknowledge the Department of Geoscience and Petroleum at the Norwegian University of Science and Technology for funding the work. We thank the Norwegian Research Council and the industry partners of the GAMES consortium at NTNU for financial support with regard to publication (grant no. 294404). We thank M. Dietrich for providing his reflectivity code, SKB2. We also thank the reviewers for their comments and suggestions that improved this work.

DATA AND MATERIALS AVAILABILITY

All the data we have used in our research work is publicly available from the Norwegian Petroleum Directorate (NPD) via their DISKOS database.

APPENDIX A

SUMMARY OF STATISTICAL REGRESSION METHODS USED

Drift gradients and uncertainties on them were estimated via χ^2 minimization. This is an approach that allows the assignment of an approximate error bar on the gradient in the absence of estimates of the measurement errors (Press et al., 1992).

The weighted least-squares nonlinear regression used to produce the model described by equation 5 and displayed in Figure 5 was produced using a weighted nonlinear least-squares regression carried out in the "stats" package in the statistical analysis software R (R Core Team, 2018). The Gauss-Newton method was used based on starting values for our three parameters of $a_0 = 0.01\,\mathrm{s}^2/\mathrm{m}^2$, $V_{\mathrm{P1}} = 1550$ m/s, and $V_{\mathrm{P2}} = 5000$ m/s. The weights used in the regression were the reciprocals of the variances in Q^{-1} produced from the procedure based on χ^2 minimization, documented above. Confidence intervals on model parameters were derived based on the delta method.

APPENDIX B

PROPAGATION OF ERRORS FORMULAS

Equation B-1 is a common method for computing the total uncertainty in a quantity that is a function of more than one variable (Lyons, 1991). The variance on a quantity $Z = f(x_1, x_2, \ldots, x_n)$ assuming that each variable x_i has its own Gaussian random error σ_i, which is relatively small, and that the errors on the variables are uncorrelated, can then be computed by

$$\sigma_z^2 \approx \sum_{i=1}^{n} \left(\frac{\partial z}{\partial x_i}\right)^2 \cdot \sigma_{x_i}^2. \qquad \text{(B-1)}$$

Applying this general formula to equation 2 gives

$$\sigma_{(Q^{-1})}^2 \approx \left[\frac{\pi V_{\mathrm{P0}f2}}{\ln\left(\frac{f_2}{f_1}\right)\left(V_{\mathrm{P0}f2}\frac{\Delta\mathrm{drift}}{\Delta z}+1\right)^2}\right]^2 \cdot \sigma_{\frac{\Delta\mathrm{drift}}{\Delta z}}^2 + \left[\frac{\pi\frac{\Delta\mathrm{drift}}{\Delta z}}{\ln\left(\frac{f_2}{f_1}\right)\left(V_{\mathrm{P0}f2}\frac{\Delta\mathrm{drift}}{\Delta z}+1\right)^2}\right]^2 \cdot \sigma_{V_{\mathrm{P0}f2}}^2 + \left[\frac{\pi\left(\frac{1}{V_{\mathrm{P0}f2}\frac{\Delta\mathrm{drift}}{\Delta z}+1}-1\right)}{\frac{f_2}{f_1}\left(\ln\left(\frac{f_2}{f_1}\right)\right)^2}\right]^2 \cdot \sigma_{\frac{f_2}{f_1}}^2. \qquad \text{(B-2)}$$

Assuming that the frequency ratio (f_2/f_1) is known and constant and that the variance $\sigma_{(V_{\mathrm{P0}f2})}^2$ on the integrated sonic velocity is relatively small, we can neglect the second and third terms in equation B-2 to approximate the variance on Q^{-1} as

$$\sigma_{(Q^{-1})}^2 \approx \left[\frac{\pi V_{\mathrm{P0}f2}}{\ln\left(\frac{f_2}{f_1}\right)\left(V_{\mathrm{P0}f2}\frac{\Delta\mathrm{drift}}{\Delta z}+1\right)^2}\right]^2 \cdot \sigma_{\frac{\Delta\mathrm{drift}}{\Delta z}}^2. \qquad \text{(B-3)}$$

APPENDIX C

DATA SELECTION AND EXCLUSION

It is important to be clear about the reasons for exclusion of any data from an analysis. For inclusion in our regression analysis, drift values from a particular interval were assessed against a set of objective criteria. Table C-1 lists the North Sea wells analyzed, as well as those that were fully or partially excluded from our regression analysis, along with the criteria for exclusion in each case. For discussion of the many potential nondispersive causes of drift, including causes of negative drift, see Stewart et al. (1984) and Goetz et al. (1979). Note that almost all wells contained at least one interval excluded from the analysis; this is mostly due to the presence of distinct geologic groups that are too thin to analyze in each well.

Given the exploratory nature of this study and the limitation to publicly released data, it was not practicable to investigate all of these problematic wells and zones in detail. With careful petrophysical analysis, it may be possible to edit some of these zones such that they could be included in the study.

Table C-1. Wells and intervals included and excluded from the study. Inclusion/exclusion criteria: (1) the drift gradient must be positive, (2) the interval must contain at least three points on the time-depth curve, (3) the measurement interval must span at least 250 m, (4) the interval used must contain a single dominant linear trend without a clear systematic curvature or multiple linear segments, and (5) adverse borehole conditions.

Well name	Inclusion (I), full (F), or partial (P) exclusion?	Reason(s) for exclusion by group. Groups: All (A), Nordland (N), Hordaland (Ho), Rogaland (R), Shetland (Sh), Cromer-Knoll (CK), Viking (V), Brent (B), Dunlin (D), Statfjord (St), Hegre (He)
15/9-6	F	A — well excluded due to predominantly negative drift
24/6-1	F	A — well excluded due to suspicious misalignment of drift gradients and formation tops
25/11-15	P	N(1) R(3,4,5) Sh(1,3) V(3)
30/6-1	P	Ho(1) R(3) Sh(2,3)
30/6-8	P	N(2) R(2) Sh(2,3) B(2,3)
31/2-6	P	V(1,4,5)
33/5-2	P	N(2) CK(2,3,5) V(3) B(3)
34/2-2R	P	N(2,4) Ho(2,3) R(2,3) CK(3) V(2,3) D(2) St(2,3)
34/7-1	I	
34/7-2	P	Ho(3) R(3) D(3) He(3)
34/7-5	P	R(3,4) B(1,3)
34/7-6	P	N(3) R(1,3,4) D(3)
34/7-12	P	R(3) B(1,3) St(3)
34/8-1	P	R(3) B(1,3) D(1) St(3) He(3)
34/8-6	P (blind well)	R(3) V(3) B(3) Ho and Sh ok, but not included in the regression, as it is the blind well
35/3-2	P	Ho(1,3) R(1,3) N(4) D(2,3)
35/11-1	P	Ho(2,3) R(1) B(3) St(1) H(3)

REFERENCES

Aki, K., and P. G. Richards, 1980, Quantitative seismology — Theory and methods: W. H. Freeman.

Batzle, M. L., D.-H. Han, and R. Hofmann, 2006, Fluid mobility and frequency-dependent seismic velocity — Direct measurements: Geophysics, **71**, no. 1, N1–N9, doi: 10.1190/1.2159053.

Beckwith, J., R. Clark, and L. Hodgson, 2017, Estimating frequency-dependent attenuation quality factor values from prestack surface seismic data: Geophysics, **82**, no. 1, O11–O22, doi: 10.1190/geo2016-0169.1.

Beckwith, J. A., 2017, Constant and frequency-dependent seismic quality factors measured from surface and borehole seismic surveys: Ph.D. thesis, University of Leeds.

Carcione, J. M., and H. B. Helle, 2002, Rock physics of geopressure and prediction of abnormal pore fluid pressures using seismic data — Part 1: Canadian Society of Exploration Geophysicists Recorder, **27**, 8–32.

De, G. S., D. F. Winterstein, and M. A. Meadows, 1994, Comparison of P- and S-wave velocities and Q's from VSP and sonic log data: Geophysics, **59**, 1512–1529, doi: 10.1190/1.1443541.

Dietrich, M., 1988, Modeling of marine seismic profiles in the t-x and tau-p domains: Geophysics, **53**, 453–465, doi: 10.1190/1.1442477.

Dutta, N., and A. Seriff, 1979, On White's model of attenuation in rocks with partial gas saturation: Geophysics, **44**, 1806–1812, doi: 10.1190/1.1440940.

Evans, D., 2003, The millennium atlas: Petroleum geology of the central and northern North Sea: The Geological Society of London.

Futterman, W. I., 1962, Dispersive body waves: Journal of Geophysical Research, **67**, 5279–5291, doi: 10.1029/JZ067i013p05279.

Goetz, J. F., L. Dupal, and J. Bowler, 1979, An investigation into discrepancies between sonic log and seismic check shot velocities: Journal of the Australian Petroleum Exploration Association, **19**, 131–141, doi: 10.1071/AJ78014.

Gurevich, B., and R. Pevzner, 2015, How frequency dependency of Q affects spectral ratio estimates: Geophysics, **80**, no. 2, A39–A44, doi: 10.1190/geo2014-0418.1.

Houck, R. T., 1987, Comparison of Q measurements from logs and VSPs: 57th Annual International Meeting, SEG, Expanded Abstracts, 786–788, doi: 10.1190/1.1891958.

Isaksen, D. and K. Tonstad, eds., 1989, A revised Cretaceous and Tertiary lithostratigraphic nomenclature for the Norwegian North Sea: Norwegian Petroleum Directorate Bulletin, **5**, 1–59.

Klimentos, T., 1995, Attenuation of P- and S-waves as a method of distinguishing gas and condensate from oil and water: Geophysics, **60**, 447–458, doi: 10.1190/1.1443782.

Koesoemadinata, A. P., and G. A. McMechan, 2001, Empirical estimation of viscoelastic seismic parameters from petrophysical properties of sandstone: Geophysics, **66**, 1457–1470, doi: 10.1190/1.1487091.

Kolsky, H., 1956, The propagation of stress pulses in viscoelastic solids: Philosophical Magazine, **1**, 693–710, doi: 10.1080/14786435608238144.

Liu, H.-P., H. Kanamori, and D. L. Anderson, 1976, Velocity dispersion due to anelasticity; implications for seismology and mantle composition: Geophysical Journal of the Royal Astronomical Society, **47**, 41–58, doi: 10.1111/j.1365-246X.1976.tb01261.x.

Lyons, L., 1991, A practical guide to data analysis for physical science students: Cambridge University Press.

Marcussen, Ø., B. I. Thyberg, C. Peltonen, J. Jahren, K. Bjørlykke, and J. I. Faleide, 2009, Physical properties of Cenozoic mudstones from the northern North Sea: Impact of clay mineralogy on compaction trends: AAPG Bulletin, **93**, 127–150, doi: 10.1306/08220808044.

Mondol, N. H., K. Bjørlykke, J. Jahren, and K. Høeg, 2007, Experimental mechanical compaction of clay mineral aggregates — Changes in physical properties of mudstones during burial: Marine and Petroleum Geology, **24**, 289–311, doi: 10.1016/j.marpetgeo.2007.03.006.

Neep, J. P., 1995, Robust estimation of P-wave attenuation from full waveform array sonic data: Journal of Seismic Exploration, **4**, 329–344.

O'Doherty, R. F., and N. A. Anstey, 1971, Reflections on amplitudes: Geophysical Prospecting, **19**, 430–458, doi: 10.1111/j.1365-2478.1971.tb00610.x.

Øygarden, B., H. Løseth, and S. Njerve, 2015, Rock properties of smectite- and ooze-rich claystones: Geophysics, **80**, no. 1, D89–D98, doi: 10.1190/geo2013-0363.1.

Pinson, L. J. W., T. J. Henstock, J. K. Dix, and J. M. Bull, 2008, Estimating quality factor and mean grain size of sediments from high-resolution marine seismic data: Geophysics, **73**, no. 4, G19–G28, doi: 10.1190/1.2937171.

Press, W. H., S. A. Teukolsky, W. T. Vetterling, and B. P. Flannery, 1992, Numerical recipes in Fortran 77 — The art of scientific computing, 2nd ed.: Cambridge University Press.

R Core Team, 2018, R: A language and environment for statistical computing: R Foundation for Statistical Computing.

Raikes, S. A., and R. E. White, 1984, Measurements of earth attenuation from downhole and surface seismic recordings: Geophysical Prospecting, **32**, 892–919, doi: 10.1111/j.1365-2478.1984.tb00745.x.

Rappin, D., and C. Barnes, 2008, Contribution to the understanding of field-specific seismic attenuation: 78th Annual International Meeting, SEG, Expanded Abstracts, 1830–1834, doi: 10.1190/1.3059257.

Richards, P. G., and W. Menke, 1983, The apparent attenuation of a scattering medium: Bulletin of the Seismological Society of America, **73**, 1005–1021.

Rickett, J., 2007, Estimating attenuation and the relative information content of amplitude and phase spectra: Geophysics, **72**, no. 1, R19–R27, doi: 10.1190/1.2399451.

Sato, S., H. Yamamoto, and D. Cao, 2000, Can discrepancy between seismic and sonic transit times be modeled?: Presented at the 6th Well Logging Symposium of Japan, SPWLA.

Stewart, R. R., P. D. Huddlestone, and T. K. Kan, 1984, Seismic versus sonic velocities: A vertical seismic profiling study: Geophysics, **49**, 1153–1168, doi: 10.1190/1.1441745.

Storvoll, V., K. Bjørlykke, and N. H. Mondol, 2005, Velocity-depth trends in Cenozoic sediments from the Norwegian Shelf: AAPG Bulletin, **89**, 359–381, doi: 10.1306/09290505084.

Strick, E., 1971, An explanation of observed time discrepancies between continuous and conventional well velocity surveys: Geophysics, **36**, 285–295, doi: 10.1190/1.1440169.

Strijbos, F., C. V. Eden, and R. Baseliers, 1998, Matching two worlds: Deabsorption of seismic data: 1998 PETEX Conference, London, PESGB, Expanded Abstracts, L7.

Tezuka, K., and A. Takahashi, 1993, Discrepancies between sonic log and VSP velocities in volcanic rocks: 63rd Annual International Meeting, SEG, Expanded Abstracts, 715–718, doi: 10.1190/1.1822597.

Thyberg, B., J. Jahren, T. Winje, K. Bjørlykke, J. I. Faleide, and Ø. Marcussen, 2010, Quartz cementation in Late Cretaceous mudstones, northern North Sea: Changes in rock properties due to dissolution of smectite and precipitation of micro-quartz crystals: Marine and Petroleum Geology, **27**, 1752–1764.

Thyberg, B. I., H. Jordt, K. Bjørlykke, and J. I. Faleide, 2000, Relationships between sequence stratigraphy, mineralogy and geochemistry in Cenozoic sediments of the northern North Sea, Dynamics of the Norwegian margin: Geological Society, 245–272 (Special Publication no. 167), doi: 10.1144/GSL.SP.2000.167.01.10.

Toverud, T., and B. Ursin, 2005, Comparison of seismic attenuation models using zero-offset vertical seismic profiling (VSP) data: Geophysics, **70**, no. 2, F17–F25, doi: 10.1190/1.1884827.

van der Baan, M., 2002, Constant Q and a fractal, stratified Earth: Pure and Applied Geophysics, **159**, 1707–1718, doi: 10.1007/s00024-002-8704-0.

Vigner, A. K., M. Deighton, and C. Swift, 2010, Q estimation on conventional and dual-sensor systems: 72nd Annual International Conference and Exhibition, EAGE, Extended Abstracts, G022.

Waters, K. H., 1981, Reflection seismology: A tool for energy resource exploration, 2nd ed.: Wiley.

Wensaas, L., H. Shaw, K. Gibbons, P. Aagaard, and H. Dypvik, 1994, Nature and causes of overpressuring in mudrocks of the Gullfaks area, North Sea: Clay Minerals, **29**, 439–449, doi: 10.1180/claymin.1994.029.4.04.

White, J., 1975, Computed seismic speeds and attenuation in rocks with partial gas saturation: Geophysics, **40**, 224–232, doi: 10.1190/1.1440520.

White, R. E., 1992, The accuracy of estimating Q from seismic data: Geophysics, **57**, 1508–1511, doi: 10.1190/1.1443218.

Worthington, M. H., and J. A. Hudson, 2000, Fault properties from seismic Q: Geophysical Journal International, **143**, 937–944, doi: 10.1046/j.1365-246X.2000.00315.x.

Zhou, J.-X., X.-Z. Zhang, and D. P. Knobles, 2009, Low-frequency geoacoustic model for the effective properties of sandy seabottoms: Journal of the Acoustical Society of America, **125**, 2847, doi: 10.1121/1.3089218.